**ORIGINAL ARTICLE**

# Laser-induced softening analysis of a hardened aluminum alloy by physical simulation

**Maria Emanuela Palmieri [1] · Vincenzo Domenico Lorusso [1] · Luigi Tricarico [1]**

**Abstract**

The study focuses on the analysis of the softening effects of the work-hardened aluminum alloy sheets EN AW 5754 H32 1.5 mm thick, through the physical simulation of thermal cycles induced in the material by laser heat treatments (LHTs). A numerical-experimental approach was implemented to define the laser thermal cycles and to subsequently reproduce them on the Gleeble™ 3180 physical simulator. The obtained softening was measured by microhardness and metallographic analysis tests. For the definition of laser thermal cycles, preliminary tests with a 2.5 kW $CO_2$ laser source have been realized, and a three-dimensional transient finite element thermal models were developed and calibrated with the experimental results. The investigated laser heat treatment parameters explored thermal cycles with different shape, interaction time, and peak temperature. Physical simulation tests were performed using laser thermal cycles that showed the maximum softening of the aluminum alloy. A three-dimensional transient finite element thermoelectric model was developed to design the shape of the Gleeble specimens, which satisfy the heating and cooling rate required by laser thermal cycles. Results obtained show that it is possible to physically simulate the investigated laser thermal cycles, reducing the cross section of the shaped part of the specimen. Softening effects depend on the thermal cycle shape. Greater softening is observed by increasing the interaction time and the peak temperature, but beyond a peak temperature threshold value, negligible effects are detected.

**Keywords** Laser methods · Aluminum alloys · Physical simulation · Finite element analysis · Hardness

## 1 Introduction

Interest in the local softening using laser heat treatment process is growing in recent period because it offers the possibility to process metal alloy sheets locally, creating areas with defined mechanical properties. This treatment is increasingly used in the local softening of high-strength steel sheet parts facilitating riveting phase in the treated areas [1] or in the local softening of high-strength aluminum alloys (work hardened or age hardenable) [2, 3], improving their formability before

✉ Maria Emanuela Palmieri
  mariaemanuela.palmieri@poliba.it

  Vincenzo Domenico Lorusso
  vincenzodomenico.lorusso@poliba.it

  Luigi Tricarico
  luigi.tricarico@poliba.it

[1]  Dipartimento di Meccanica, Matematica e Management, Politecnico di Bari, Via E. Orabona 4, 70125 Bari, Italy

forming. In this latter process, also known as Tailored Heat Treated Blank (THTB), the laser heat treatment enables the local tailoring of the material properties [4]. The biggest challenge for the successful production of THTB is the definition of an appropriate heat treatment layout [5]. It is necessary to evaluate the influence of laser thermal cycles on the material properties, making careful assessments of the process parameters before starting a process on an industrial scale. For this purpose, physical simulators such as Gleeble systems allow to reproduce thermomechanical cycles typical of manufacturing processes, also in the severe condition realized by laser heat treatments (thermal cycles with higher heating and cooling rate). It is thus possible to predict in a laboratory scale how the mechanical properties of materials are influenced and also avoiding problems encountered during a real industrial process. For example, laser heat treatments can lead to distortion phenomena that can be avoided by using Gleeble system, thus obtaining more correct evaluations.

The physical simulation was designed for the reproduction of situation occurring in material affected by heat generated during welding. In particular, a Gleeble system has been used
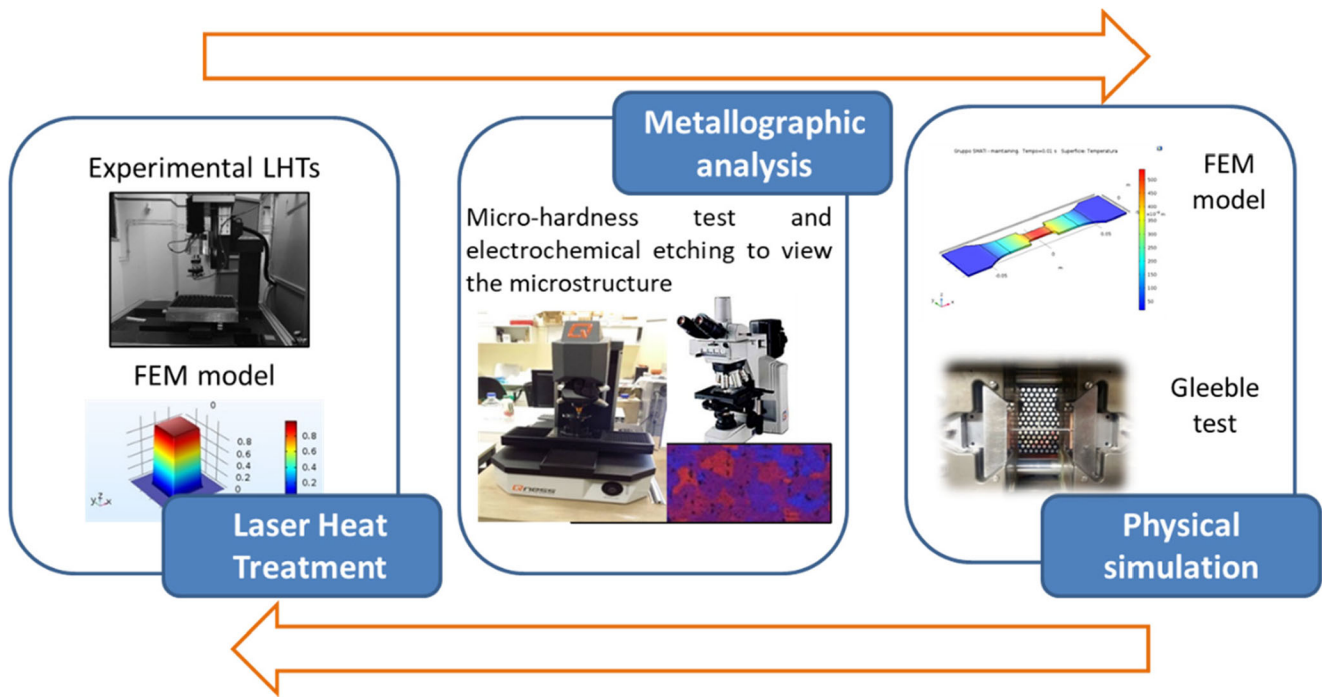
**Fig. 1** Scheme of adopted methodology

to control thermal cycles in TIG welding of Inconel alloys, evaluating the effects in terms of microstructure and mechanical properties [6]. In other studies, a Gleeble system was used to determine the effects of different cooling times on the microstructure of HAZ (heat-affected zone). Into one of these, a special drilled bar specimen with external cooling was used to physically simulate gas metal arc welding technology [7]. For the same problem, a special isothermal quenching cylindrical device (ISO-QTM) was adopted to test the HAZ during laser welding [8]. These studies highlight that Gleeble systems have no problem to guarantee heating rate up to $10^3$K/s [9], thanks to the AC electric resistance heating system. On the contrary, the achievable cooling rates by the water-cooled jaws surrounding the specimen and the eventually additional presence of external cooling can be insufficient with respect to those required, especially for the severe thermal cycles induced by laser. Special specimen geometries, such as ISO-QTM and special drilled bars, are solution examples, which allow

increasing the cooling rate for not flat specimens. On flat specimens, the increase of cooling rate was investigated by reducing the specimen cross section [10].

This paper illustrates a numerical-experimental methodology to physically simulate thermal cycles obtained by laser heat treatment and to obtain a correlation between laser parameters and the softening level. The methodology was implemented on the work-hardened aluminum alloy sheet EN AW 5754 H32 with a thickness of 1.5 mm, to improve the formability of the treated areas. A preliminary experimentation, performed with a $CO_2$ laser source, allowed to calibrate two thermal 3D FE models and to define the thermal cycles varying laser parameters. Some thermal cycles were then physically simulated with the Gleeble 3180$^{TM}$ system using original specimens able to realize in the specimen the high cooling rate induced by laser treatment; a thermoelectric 3D FE model has been designed to define specimen shape and size. Considerations on softening phenomena were taken,

**Fig. 2** **a** Numerical-experimental comparison of the thermal cycle in the PM treatment realized with a laser power of 1.0 kW and a treatment speed of 7.5 mm/s. **b** Numerical-experimental comparison of the thermal cycle in the PM treatment realized with a laser power of 0.5 kW and a pulse time of 6 s
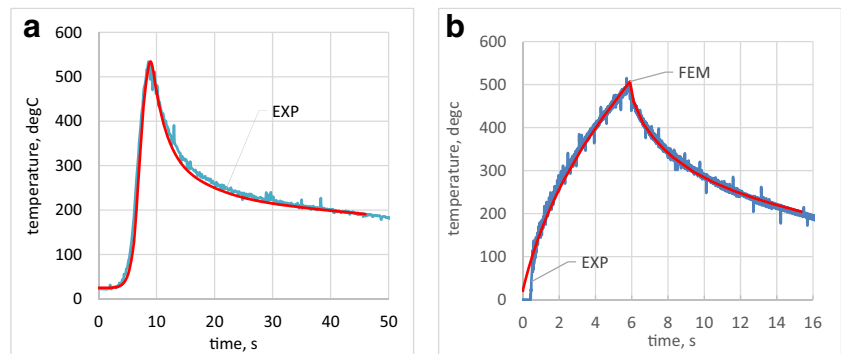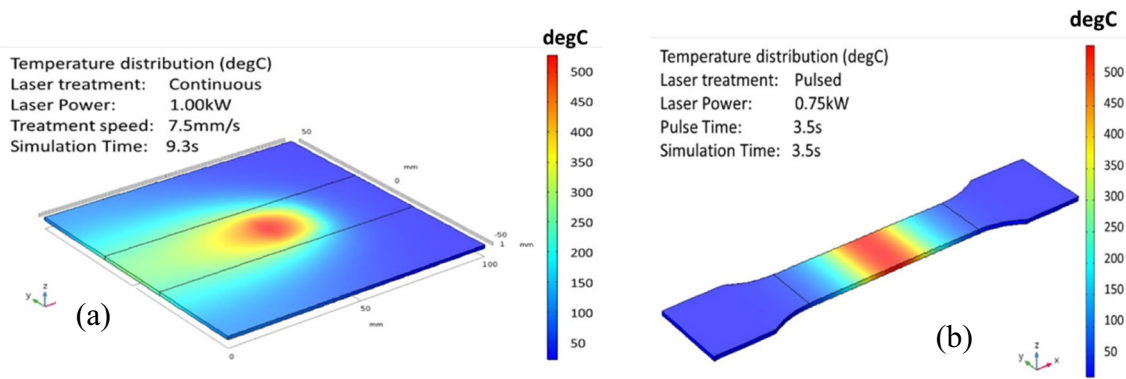
**Fig. 3** Temperature distribution in the FE simulation of the CM laser surface treatment, when the laser beam is in the specimen center (**a**) and of PM laser surface treatment at the end of the pulse time (**b**)

thanks to the analysis of numerical and experimental results obtained from metallographic analyses on Gleeble specimens.

## 2 Material and methods

This work deals with the study of the softening effects induced by laser heat treatments (LHTs) on the EN AW 5754 H32 aluminum alloy 1.5 mm thick with a hardness of 81HV0.2 in the conditions received, through physical simulation tests. The adopted methodology is outlined in Fig. 1 and includes laser heat treatment for the acquisition of thermal cycles and the process modeling, physical simulation of laser thermal cycles, and metallographic analysis for the softening assessment of the specimens treated by laser and physical simulation.

In particular, (i) the laser heat treatment was carried out with an experimental numerical approach. Preliminary tests with $CO_2$ lasers were performed on specimens of suitable geometry (laser specimens), acquiring some thermal cycles obtained by varying treatment conditions and process parameters; for each treatment condition, laser tests were used to calibrate a 3D transient finite element (FE) thermal model. By combining the results of the physical simulation and the metallographic analysis, the FE model was used to estimate the aluminum alloy softening according to the treatment conditions and the laser process parameters. (ii) The physical

simulation of the acquired thermal cycles was performed with an experimental numerical approach. A 3D transient finite element thermoelectric model was developed for the design of the physical simulation tests, defining the shape and size of the specimens that allow the high cooling rates of the laser thermal cycles. The physical simulation tests were carried out with the Gleeble 3180 system for some of the thermal cycles acquired with laser thermal treatments. (iii) The metallographic analysis was performed with microhardness tests on laser and Gleeble specimens to evaluate the softening effects induced by thermal cycles; electrochemical etching tests were performed to analyze the effect of heat treatments on the grain size.

### 2.1 Definition of laser thermal cycles

#### 2.1.1 Laser surface treatments

Laser surface treatments were realized using a 2.5 kW $CO_2$ laser source. An optical lens with a focal length equal to 225 mm was used, allowing a defocused laser beam with a square spot area (400 $mm^2$) and a top-hat intensity distribution. To increase the absorption of laser radiation, specimens were coated with colloidal graphite before laser treatments. LHTs were performed moving the laser source with a constant treatment speed (continuous mode, CM) and with the laser source stationary with respect to the specimen surface (pulsed



**Fig. 4** **a** Peak temperature versus pulse time, obtained in the simulation of the PM laser surface treatment at different laser power. **b** Peak temperature versus laser power obtained in the simulation of PM laser surface treatment, at different pulse time
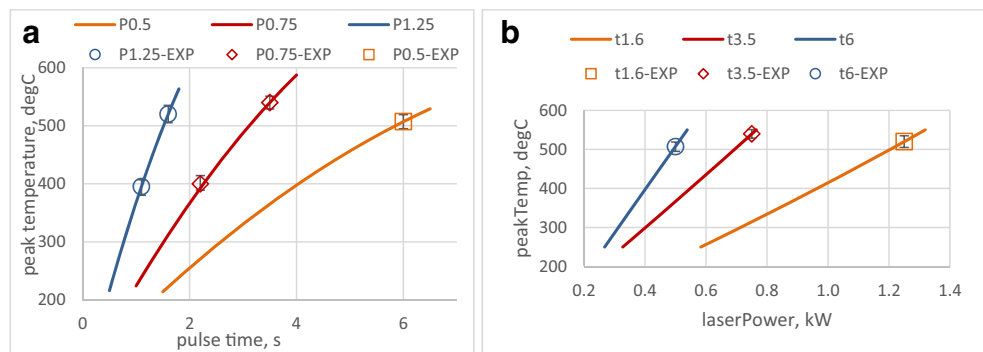
**Fig. 5 a** Peak temperature versus treatment speed obtained in the simulation of the CM laser surface treatment at different laser power. **b** Peak temperature versus laser power obtained in the simulation of the CM laser surface treatment at different treatment speed
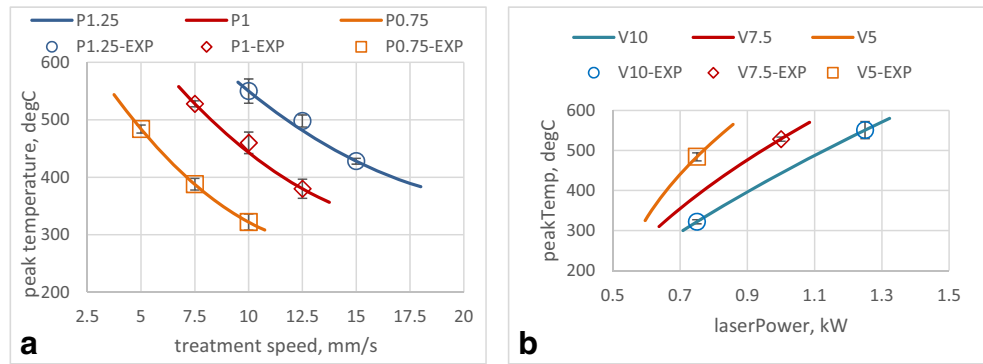


mode, PM). In the CM, the laser source trajectory coincides with the center line of a 100 × 100-mm square specimen, while in the PM, the laser source radiates for a given pulse time the center of a rectangular 100 × 20-mm sample. During the laser surface treatments, a k-type thermocouple has been used for the acquisition of the thermal cycles. This was welded before treatment in the center of the lower side (the side not exposed to laser radiation) of the square and rectangular samples. LHTs were performed varying the laser power ($P$) and the treatment speed ($V$) or the pulse time ($t$).

### 2.1.2 Numerical simulation of laser surface treatment

With the aim to perform a deeper investigation of the effects of laser process parameters on specimen temperature distribution and on thermal cycles in some points of the specimens, a 3D transient finite element thermal model has been developed for the CM and PM laser surface treatment simulation. The FE model was implemented using Comsol Multiphysics. The 20 × 20-mm laser source has been modeled as a surface thermal flux with a top-hat distribution. In continuous mode treatment, the laser source moves with a constant laser treatment speed, while in pulsed mode, the laser source is active for time shorter than the pulse time. The thermo-physical parameters were modeled as a function of temperature. Heat loss from the sample surfaces was modeled with a constant convective heat transfer coefficient. Using the thermal cycles acquired in the experimental tests, the calibration of the FE model was obtained by defining the convective heat transfer coefficient and a

laser source absorption coefficient, which delimits the portion of the laser power supplied to the specimen.

The numerical-experimental comparison of thermal cycles highlighted in Fig. 2a and b shows the results of this calibration phase for two of the process conditions investigated in PM and CM laser surface treatment. It is possible to observe that the numerical curves are in good agreement with the experimental ones.

As example of FE model simulation results, Fig. 3 shows the temperature distribution obtained respectively: (i) when the laser source is on the specimen center in the CM laser surface treatment (Fig. 3a) (ii) and at the end of the pulse time in the PM treatment simulation (Fig. 3b). Due to the reduced thickness of the specimens, the difference in temperature between top (the surface of the specimen irradiated by the laser) and bottom side is a few Celsius degrees.

The process window investigated was determined, thanks to preliminary experimental tests. The power and interaction time parameters have been varied in order to obtain peak temperatures between 450 and 500 °C. The laser conditions explored are those which allow to obtain the aluminum alloy softening. Figures 4 and 5 synthetize the process window investigated for the two different laser surface treatments. In particular, Fig. 4a and b show the relationships estimated by the FE model of the peak temperature as a function of the pulse time and laser power, in PM laser surface treatment, while Fig. 5a and b show the relationships of the peak temperature as a function of the treatment speed and laser power, in CM laser surface treatment. Moreover, Figs. 4 and 5

**Table 1** LHT conditions

| Treatment mode | $P$ (kW) | $V$ (mm/s) | $t$ (t) | $\tau$ (s) | PT (°C) | CR (K/s) | Treatment code | Softening (%) |
|---|---|---|---|---|---|---|---|---|
| Pulsed | 0.5 | - | 6.0 | 6.00 | 507 | 105 | P0.50t6 | 93 |
| Pulsed | 0.75 | - | 3.5 | 3.50 | 540 | 170 | P0.75t3.5 | 86 |
| Pulsed | 1.25 | | 1.6 | 1.6 | 520 | 190 | P1.25t1.6 | 78 |
| Continuous | 0.75 | 5.0 | - | 4.00 | 483 | 72 | P0.75V5 | 68 |
| Continuous | 1.00 | 7.5 | - | 2.67 | 528 | 110 | P1V7.5 | 73 |
| Continuous | 1.25 | 10 | - | 2.0 | 550 | 140 | P1.25V10 | 60 |

**Fig. 6** a Thermal cycles investigated for pulsed mode treatment. **b** Thermal cycles investigated for continuous mode treatment
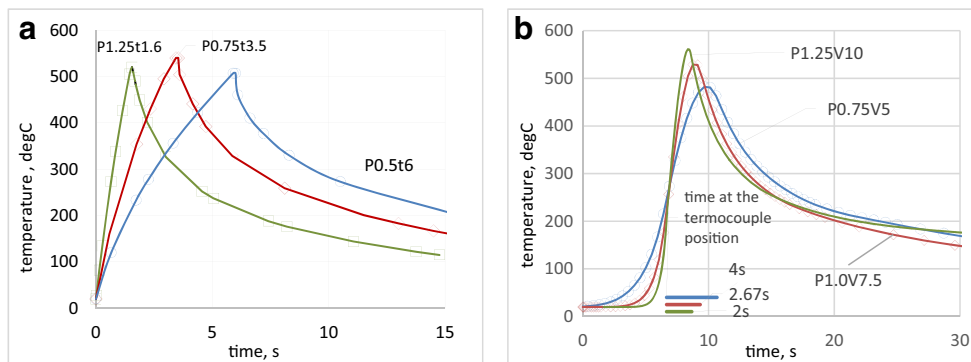


highlight the experimental results obtained in the PM and CM laser surface treatments.

### 2.1.3 Softening effects induced by laser surface treatments

At the end of the surface treatments, hardness tests were carried out in order to assess the influence of the process parameters both on the maximum lowering of material hardness and on the size of the softening zone in the specimen. Hardness results show an appreciable softening effect for peak temperatures of around 500 °C, confirming that the threshold temperature for observing appreciable softening phenomena is higher than 410 °C [3]. Furthermore, an influence of the laser interaction times ($\tau$) was observed on hardness results, where laser interaction time was assumed equal to the pulse time in the PM and equal to the ratio between laser spot size and the treatment speed in the CM treatment. Moreover, in the comparison of hardness results, the softening obtained in CM laser surface treatments highlights higher standard deviation and lower value with respect to the softening obtained in PM treatments realized with comparable peak temperatures and interaction time. At the end of the laser surface treatment, specimens treated in CM highlight higher distortions than those treated in PM.

In order to study the effect of thermal cycle on specimen without the distortion problem, a physical simulation approach was used, and three thermal cycles for each treatment mode were chosen, all characterized by a peak temperature about 500 °C and different levels of interaction time and laser power. Table 1 shows the characteristic parameters of the selected thermal cycles and the softening level reached, calculated as the ratio between the measured softening value and that associated with the complete softening condition, which is approximately 59HV0.2.

Figure 6 shows the investigated thermal cycle obtained by interpolation of acquired laser data both for the experimental pulsed mode treatment and continuous mode treatment (Fig. 6a and b, respectively). In particular, Fig. 6b shows, in addition to the interaction times of the three laser treatments, the time required for the laser beam to reach the position where the thermocouple was welded. The cycles illustrated in Fig. 6 are imposed on Gleeble system.

## 2.2 Physical simulation of laser thermal cycles

In the Gleeble 3180 system, specimens are heated by Joule effect, and a thermal cycle is reproduced in a point of the specimen (control point), modulating the current density in this point. Preliminary physical simulations of laser thermal
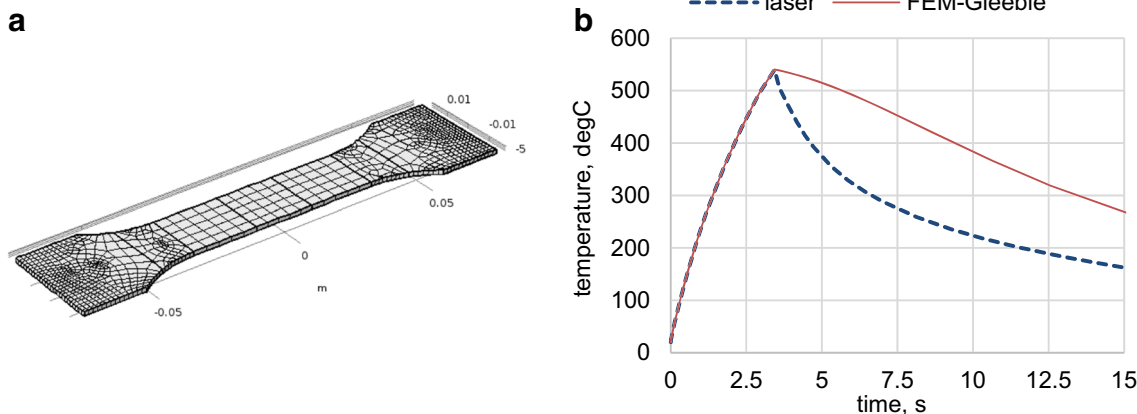


**Fig. 7** **a** Flat dog bone specimen with $L_0$ (length) of 150 mm and $W_0$ (width) of 20 mm. **b** Comparison between the laser thermal cycle and the Gleeble thermal cycle simulated with the FEM model for $P = 0.75$ kW and $\tau = 3.5$ s conditions

**Fig. 8** Geometric parameters of the Gleeble specimen
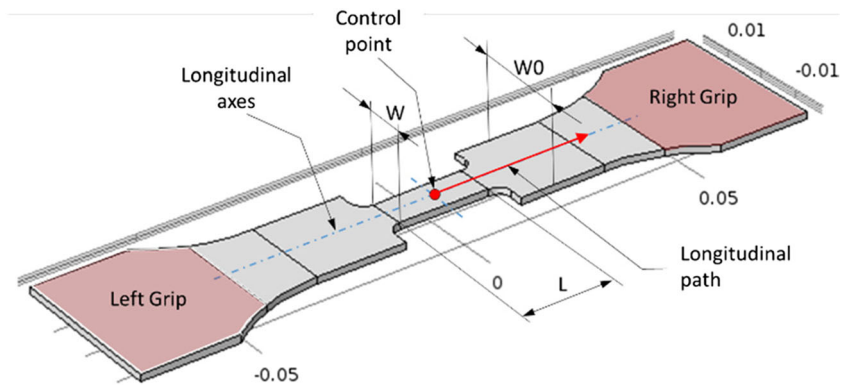


cycles using a classic flat dog bone specimen highlighted the capability of the physical simulator to reproduce in the control point only the heating phase of the thermal cycle, while cooling rates realized were lower to those induced by laser treatment. An increase of the cooling rate was observed reducing the specimen cross section in the central zone. This is because the not-shaped zone of the specimen remains at lower temperatures (lower current density) with respect to the temperatures of the shaped area (higher current density), during the heating phase; in the next cooling phase, the heat removed by conduction from the not-shaped areas of the specimen increases the cooling rates in the shaped area of the specimen.

### 2.2.1 Specimen design

A 3D transient FE thermoelectric model was developed in Comsol Multiphysics to size the shaped area of the specimen and to analyze physical simulation's results. A proportional-integrative-derivative (PID) controller was implemented in the FE model in order to guarantee the required thermal cycle in the control point [7]. The heat removed from the clamps, which are kept at a low temperature thanks to the use of a glycol solution that circulates inside them, has been modeled as heat lost by convection in the specimen gripping area.

Figure 7 highlights FE model results obtained in the simulation of the PM laser treatment with $P = 0.75$ kW and $t = 3.5$ s, when the classic flat dog bone specimen was used (Fig. 7a).

The numerical and experimental thermal cycles compared in Fig. 7b confirm the capability to reproduce the heating phase of the laser thermal cycle, as well as the difficulty to adapt the cooling phase.

Figure 8 shows the Gleeble specimen with the shaped area in the central zone. In particular, the figure highlights the length ($L$) and the width ($W$) of the shaped area, the control point, the specimen gripping areas, and the longitudinal path that was used in the post-processing phase to analyze the temperature profile at the end of the cooling phase.

A FEM simulation plan was realized, varying $L$ and $W$ parameters respectively from 15 to 25 mm and from 6 to 10 mm. In Fig. 9a and b, the temperature profiles at the end of the heating phase and the cooling curves in the control point for some combinations of $L$ and $W$ are respectively shown. It is observed that by shaping the specimen, the area subjected to high temperatures is reduced, and this leads to more drastic cooling curves. The approach allows reaching higher cooling rate than those required during the laser process, by reducing the width and/or the length of the shaped area.

The effect of the geometric parameters was investigated with kriging techniques through DACE (Design and Analysis of Computer Experiments) that is a MATLAB toolbox. A kriging approximation model based on data from a computer experiment was developed. The results are shown in Fig. 10 quantifying the effects of the shaped area parameters. Results confirm that a reduction in the width and length

**Fig. 9** **a** Temperature profiles for not-shaped (dash-dot line) and shaped specimens (solid lines). **b** Cooling curves for not-shaped (dash-dot line) and shaped specimens (solid lines). The red dashed line represents the cooling curve of laser cycle ($P = 0.75$ kW, $t = 3.5$ s)
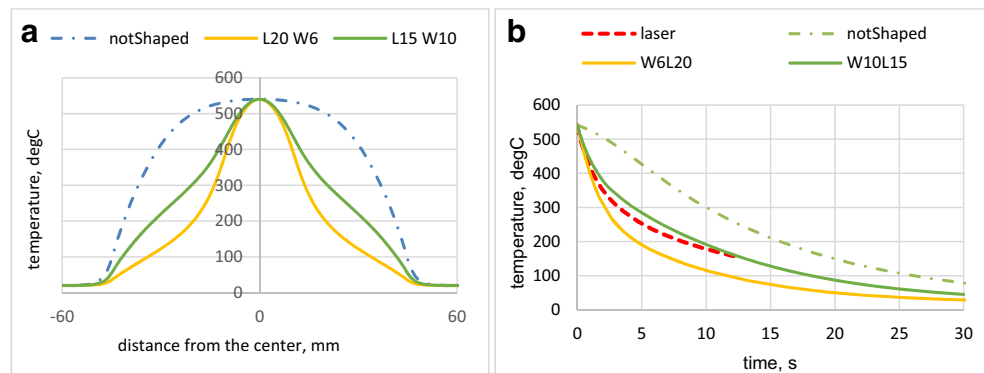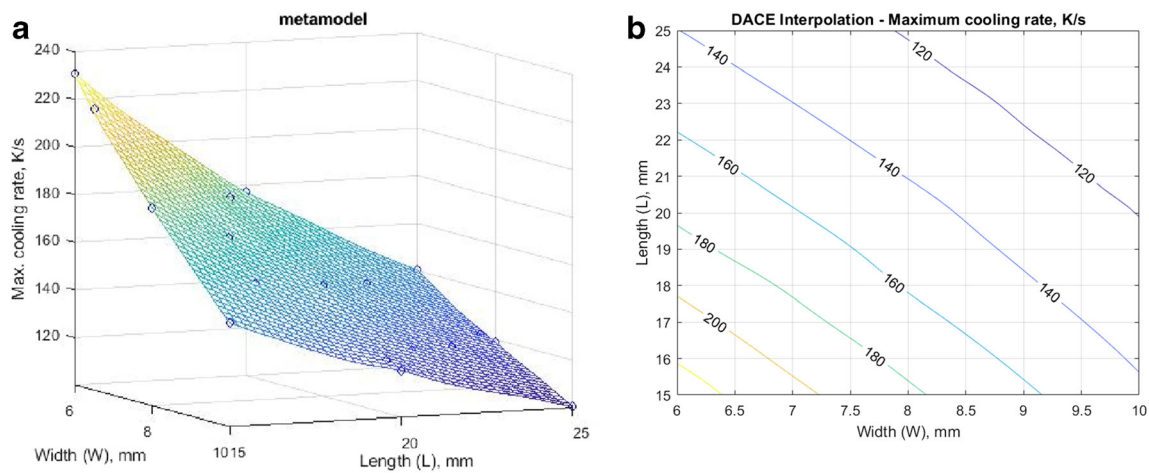
**Fig. 10** **a** Effects of the geometry of the shaped sample in terms of maximum cooling rate in the control point (response surface). **b** Effects of the geometry of the shaped sample in terms of maximum cooling rate in the control point (isolines)

of the shaped zone leads to an increase of cooling rate and that there is a greater sensitivity to the variation of $W$ rather than $L$.

### 2.2.2 Physical simulation test

The optimal specimen geometry has been designed using the results shown in Fig. 10 and the information on the maximum cooling rate required in the experimented laser treatments (Table 1). The used approach has been to create specimens with a geometry of the shaped area able to guarantee a cooling rate greater than that required in the laser thermal cycles. With this approach, it was possible to verify that the PID regulator of the Gleeble system was always able to modulate the current density both in the heating and cooling phases, perfectly reproducing the laser thermal cycles highlighted in Fig. 6. Figure 11a shows the experimental set-up for Gleeble system, while Fig. 11b shows the load unit with the specimen clamped between the grips. During the physical simulation tests, the temperature was measured by k-type thermocouples welded along the axis of the sample at points positioned 8 mm, 14 mm, and 30 mm away from the center of the

shaped section where the central thermocouple, called control point, is welded. Temperature control is based on the feedback of the latter thermocouple, which uses PID regulation. The thermal cycles measured by the thermocouples were used to calibrate the thermoelectric FE model.

### 2.2.3 Softening effects induced by physical simulation test

Once the different LHT conditions in terms of both laser power and interaction time have been physically simulated (Table 1), microhardness tests were carried out through Qness tester. The physically simulated samples were properly grinded and polished to guarantee a planar surface. Microhardness tests were realized on this surface adopting a load equal to 0.2 kg with a dwell time of 5 s. For each sample, microhardness tests were performed along the longitudinal path (Fig. 8) and along a path parallel to the previous one at 2-mm distance. For each path, microhardness test was realized with a pitch of 0.5 mm. The results of hardness profiles measured along the longitudinal path are shown in Fig. 12 for the different laser treatment condition investigated. In the shaped

**Fig. 11** **a** Experimental set-up for Gleeble system. **b** Load unit of Gleeble system
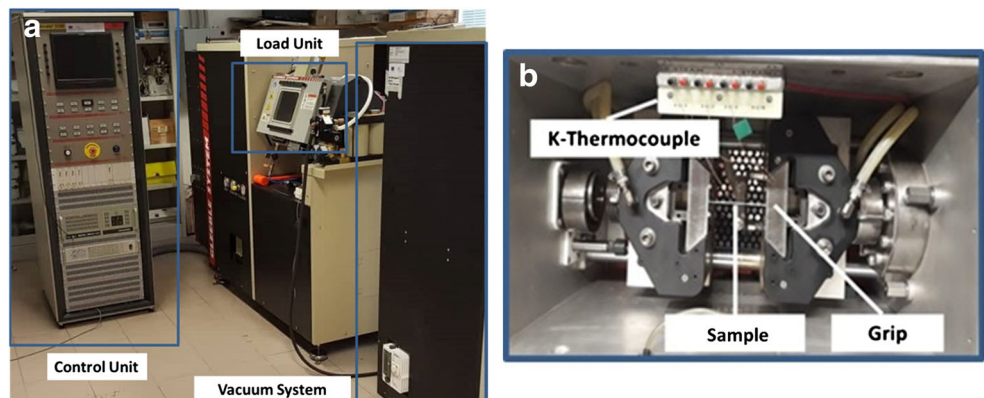
**Fig. 12** Microhardness values according to the distance from the specimen center
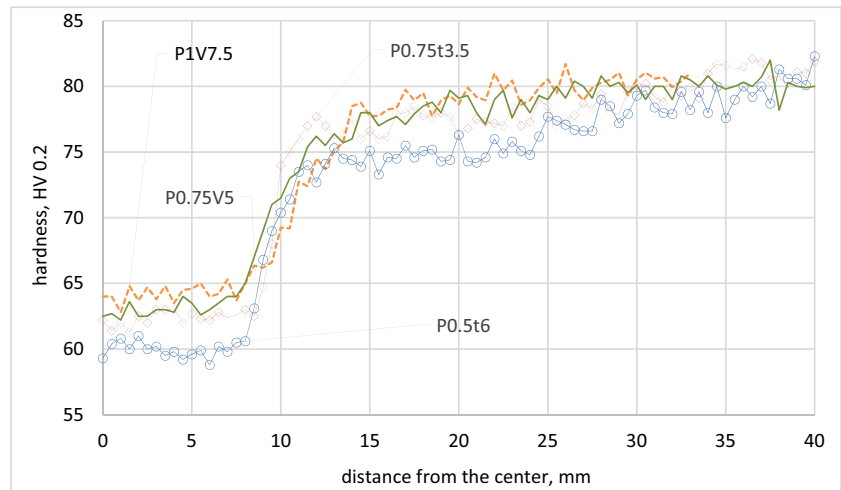


section and therefore in the section subjected to the maximum temperatures, the minimum hardness is reached; this grows up to the value at the as-received state in correspondence of the part of the specimen in contact with the cold clamps.

These results obtained by hardness analysis were confirmed observing microstructural changes in the material as a function of the distance from the specimen center and of the interaction time. An electrochemical etching procedure was performed using Barker's reagent (675 ml water, 23 ml of flour-boric acid (48%)). The anodization process was performed for 90÷120 s at 24V DC. The microstructure was possible to observe using polarized light through the Nikon Ig_ma200In optical microscope.

Considering the section of the specimen with maximum softening, it is possible to correlate the grain size and the hardness to the interaction time of the laser treatment. Figure 13a shows how the average grain size varies in the most softened stretch in the case of a PM laser treatment. Taking P0.5kWt6s as a reference, in Fig. 13b, the micrographs are respectively shown in the central zone of the shaped area and in the zone of the not-shaped area where the TC4 thermocouple was welded (30 mm from the control point). It is noted that an increase in treatment interaction time leads to an increase in grain size. For the case considered where the minimum hardness recorded in the central area is of 60 HV, there is an average grain size of 30.59 μm. This value is greater than

what is observed in the lateral area near the TC4 thermocouple. Here, the average grain size is of 15.38 μm.

## 3 Discussion

The FE thermoelectric model was employed to simulate each Gleeble tests performed. The results of physical simulations and those of numerical simulations have been compared, as highlighted in Figs. 14 and 15.

In particular, Fig. 14 shows the peak temperatures of the thermal cycles measured by the thermocouples and the profile of the peak temperatures foreseen by the FE model (obtained analyzing the thermal cycle along the longitudinal path), for the different laser conditions investigated. The same figure compares the experimental and numerical results of a not-shaped specimen in which the thermal cycle of the P0.75kW-t3.5s laser treatment is applied in the control point. These results highlight the ability of the thermoelectric FE model to estimate the actual temperature at the end of the heating phase in different thermal treatment conditions, both for the shaped and not-shaped specimens. The results also show that the effect of the specimen section reduction increases the temperature gradient along the longitudinal path.

With reference to the example case P0.75kW-V5mm/s, Fig. 15 compares the thermal cycles measured by the

**Fig. 13** **a** Average grain size in the central area depending on the interaction time of the laser treatment. **b** Microstructure 500× in central zone for 0.5 kW, 6 s (1). Microstructure 500× in lateral zone for 0.5 kW, 6 s (2)



Central area (1)

Lateral area (2)
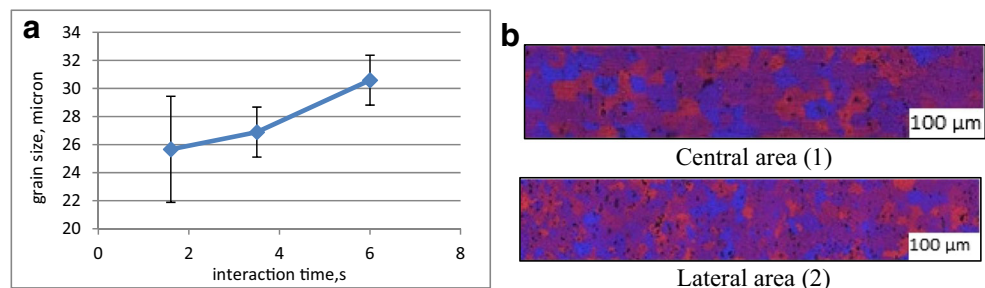
**Fig. 14** Peak temperatures of experimental (GLB label) and numerical (FEM label) thermal cycles measured/evaluated at different distances from the control point
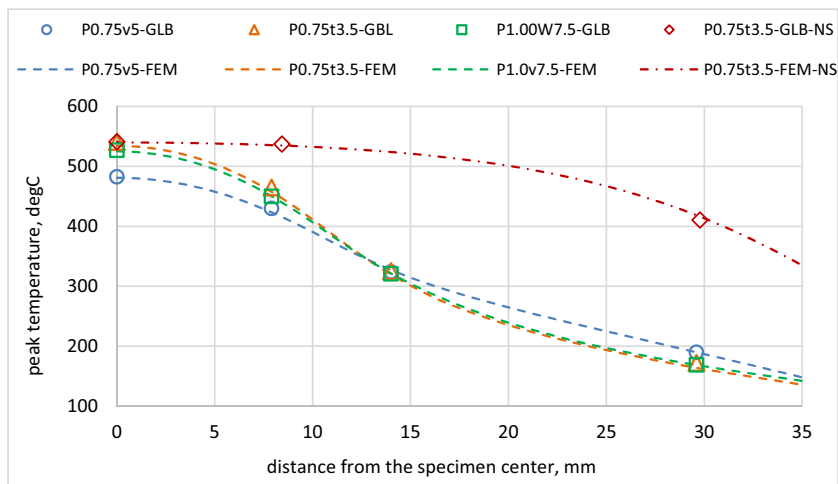


thermocouple and the numerical thermal cycles obtained from the FE model in the same points where the thermocouples were welded.

These results show the ability of the FE model to also predict the thermal cycles that are generated during the physical simulation test in the specimen points positioned at different distances from the control point; similar results were obtained by simulating other treatment conditions. Especially in the shaped zone of the specimen, the results further highlight that thermal cycles obtained at the different points of the longitudinal path have the same shape, while peak temperatures are reached at the same time. With increasing distance from the control point, a single physical simulation test is therefore able to reproduce laser thermal treatments made with the same mode (PM or CM), with the same interaction time, but with laser powers smaller than that corresponding to the control point.

The correspondence between the thermal cycles simulated in the Gleeble specimens and those obtained in the laser treatment was validated using the FE model developed to simulate the PM and CM laser treatments. The relationships shown in

Figs. 4b and 5b have been used to determine the laser power corresponding to a given peak temperature, for each treatment speed or pulse time analyzed. The shape of the thermal cycle was finally estimated with the FE model by simulating the laser treatment with the laser power and treatment speed/ pulse time previously identified. As an example, Fig. 16 shows results obtained in PM treatments performed with a pulse time of 4 s and with laser powers of 0.75 kW, 0.67 kW, and 0.59 kW.

On the basis of these considerations and using the results of the thermal FE model developed to simulate the different LHTs conditions, through the peak temperature, there exists a relationship that links the distance from the control point along the longitudinal path (Fig. 14), to the laser power for each treatment mode (Figs. 4 and 5).

Furthermore, the results of microhardness tests along the longitudinal direction of the specimen (Fig. 12) allow to create a bi-univocal correlation between the peak temperature achieved in the Gleeble test at a given point of the specimen and the corresponding hardness. Therefore, it is possible to define a direct relationship between the

**Fig. 15** Comparison between FEM and physical simulation along the longitudinal direction of the specimen for thermal cycle at different distance from the specimen center
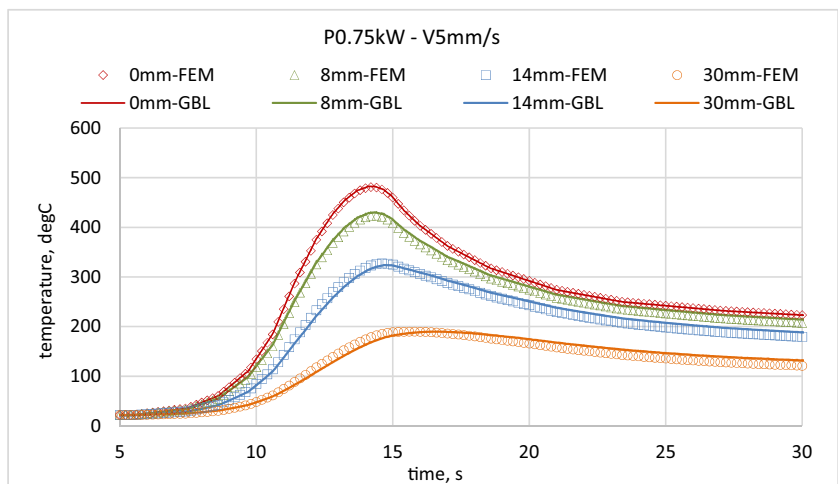
**Fig. 16** Numerical-experimental comparison of thermal cycles for laser powers 0.75 kW, 0.67 kW, and 0.59 kW
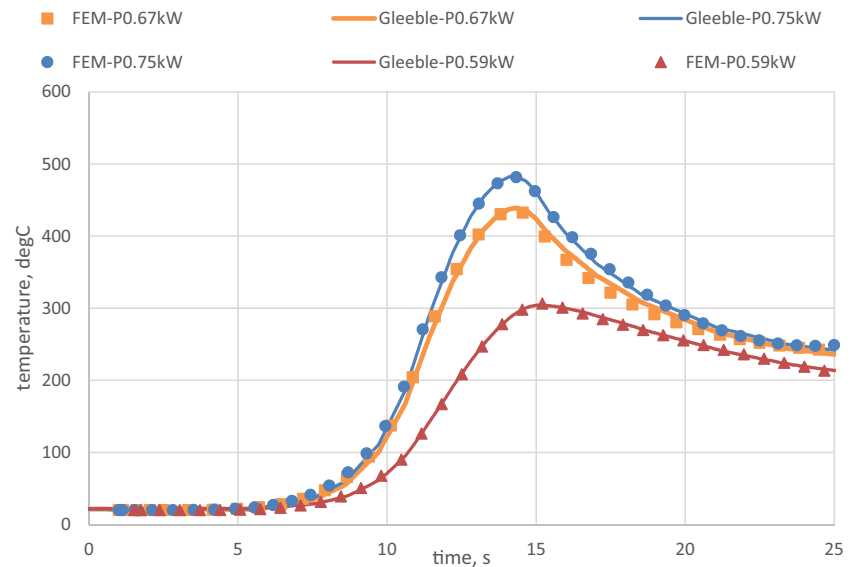


laser power and the hardness of the aluminum alloy after laser heat treatment. This relationship is made explicit with graphs proposed in Fig. 17. Specifically, Fig. 17a shows the hardness curve function of laser power for the pulsed mode treatment, and Fig. 17b shows the hardness curve function of laser power for the continuous mode treatment. For each laser treatment mode (CM or PM) and for each interaction time used (treatment speed or



**Fig. 17 a** Hardness curve function of laser power for PM treatment. **b** Hardness curve function of laser power for CM treatment

pulse time), results show that there is a threshold laser power that must be overcome to have the maximum softening of the aluminum alloy and that above this threshold power, significant variations in terms of material hardness are not appreciated. Furthermore, a reduction in the interaction time of the laser treatment leads to an increase in the threshold laser power required.

Evaluating the hardness as a function of the peak temperature for all the laser conditions investigated (Fig. 18), it is observed that below a certain peak temperature, there are no softening effects.

By increasing the peak temperature, the hardness slowly decreases in a range of peak temperatures ranging from 150 to 350 °C for longer interaction times and from 390 and 410 °C for lower interaction times.

In this range of peak temperatures (area of low softening), increasing the severity of the thermal cycle (reduction of the interaction time), a decrease in the obtainable softening is observed. Then, around between 350÷410 °C, continuing to increase the peak temperature, there is a marked reduction in hardness.

This trend is due to a first recovery phase (softening immediately after beginning the annealing) and a second recrystallization phase (subsequent acceleration in the hardness decrease). In Fig. 18, it is possible to observe that the rapidity of thermal cycles leads to an increase of beginning temperature of recrystallization, and once recrystallization was initiated, the softening rate increased significantly. The interaction time, in fact, has effects on the softening level because it postpones the recovery and recrystallization phenomena. These results are in line with those obtained in continuous heating test replicating heating rates of industrial continuous annealing of cold rolled EN AW 5754 sheet alloy [11].
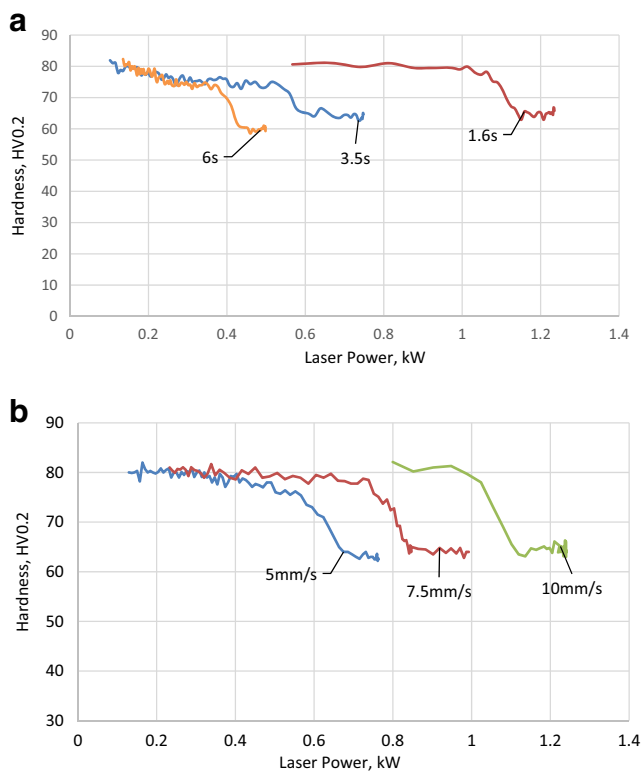
**Fig. 18** Hardness curve function of peak temperature
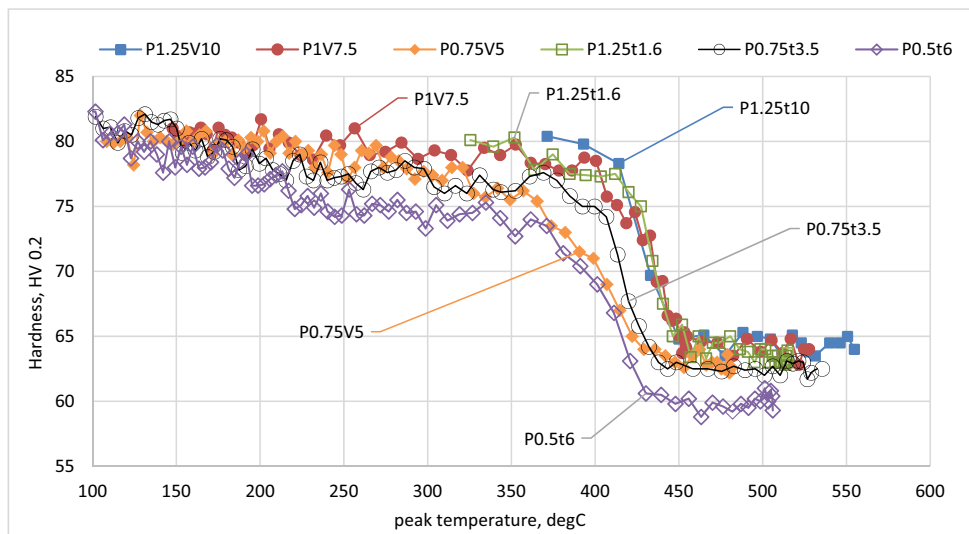


Finally, it is observed a threshold value of the peak temperature, in which the hardness reaches a minimum value; this hardness value remains constant even for thermal cycles with peak temperatures higher than the threshold temperature, defining an area of maximum softening. The severity of the thermal cycle influences the following:

The peak temperature at which the hardness begins to decrease.

The hardness at the end of low softening area.

The temperature above which the hardness decrease becomes more significant.

The threshold temperature: this increases with the increase in the severity of the thermal cycle. In the range of laser parameters examined, the maximum threshold temperature is about 450 °C and is obtained in thermal cycles performed with less interaction time.

The hardness value in the maximum softening area: the value of the minimum hardness decreases reducing the severity of the thermal cycle. The minimum hardness value is obtained in the physical simulation of the laser treatment carried out with the highest interaction time explored (6 s).

For all the laser conditions investigated, the maximum softening percentage was evaluated as a function of the interaction time. In this analysis, the mean hardness corresponding to peak temperatures above 450 °C was considered. The results are shown in Fig. 19. It can be observed that an increase in laser interaction time leads to an increase in maximum softening. Comparing the two laser treatment modes experimented, results show that for the same interaction time, the maximum softening is achieved when the heat treatment is performed in the pulsed mode on a rectangular sample. In this case, the effect of conduction is more limited because of the treatment mode and the geometry of the sample, which has width equal to the spot size. On the contrary, when the continuous treatment mode is used on a square sample, the effects of conduction are greater, and the shape of the thermal cycle changes substantially. As it is possible to appreciate in Fig. 6b, where in addition to the thermal cycles, the periods in which the laser source radiates the point where the thermocouple is welded are also highlighted, this leads to an interaction time that is lower than that theoretically calculated as ratio between treatment speed and laser spot size. Finally, by comparing the maximum softening obtained in the physical simulation tests (Fig. 12) with those obtained in the LHT (Table 1), a good correspondence is observed when the comparison is made by analyzing the pulsed treatment mode; on the contrary, the softening differences are greater in the continuous treatment mode. In these conditions, the treated samples showed distortions much greater than those of the pulsed treated samples. The distortions are probably the cause of a greater variability of the softening results due to the variation of the laser beam focus during the laser treatment. The distortion differences between the two treatment conditions investigated indicate a different thermal flux in the treated area, as confirmed observing temperature profiles along axial and transverse specimen directions (Fig. 20).
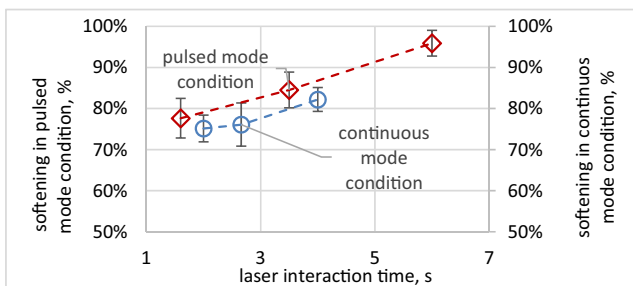


**Fig. 19** Relationship between the laser interaction time and the maximum softening

**Fig. 20** FE thermal profiles along the longitudinal and transverse axes of the specimens, simulated in the laser and physical simulation tests of the treatments P0.75kWt3.5 s (**a**) and P1kWv7.5 mm/s (**b**)
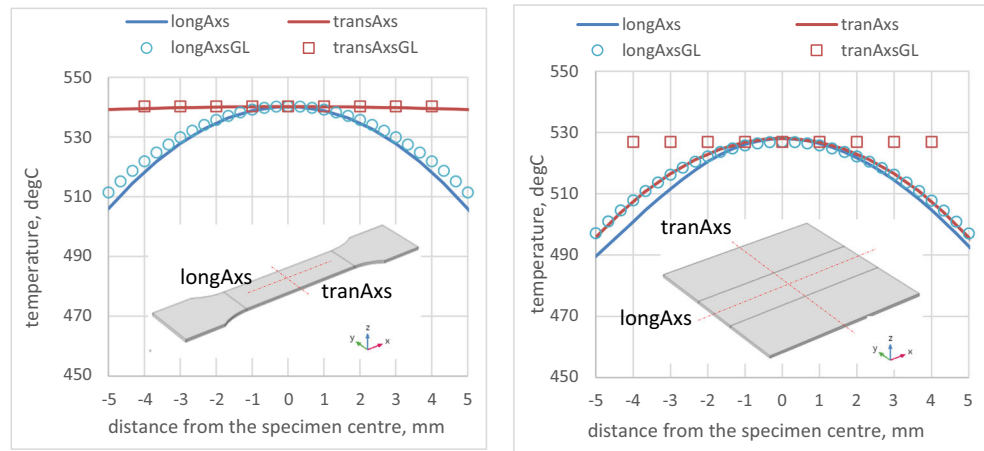


For both the PM (Fig. 20a) and CM (Fig. 20b) treatments, the profiles are obtained at the time in which the peak temperature is reached. The same figures show the longitudinal and transverse temperature profiles obtained in the Gleeble specimens as a result of physical simulation tests of PM and CM treatments. The comparison between laser heat treatment conditions shows a significant difference of the thermal gradients in the transverse direction of the specimens, which are absent in the PM treatment and comparable with that in the longitudinal direction in the CM treatment. The comparison between laser treatment and corresponding physical simulation test shows thermal gradients comparable only in the physical simulation of the PM treatment, justifying the good correspondence of the softening levels obtained (the difference in terms of softening is about 2%). There are greater differences in the physical simulation of the CM treatment (approximately 15%), highlighting how an increase in gradients in the transversal direction of the specimen reduces the level of softening possible in a CM treatment. On the one hand, this reduces the ability of the physical simulation to estimate the softening in a CM treatment, but on the other, it provides indications on the design of the heat treatment, which will have to try to reduce the gradients in the transverse direction. For example, in a single-pass treatment, this gradient reduction could be obtained by increasing the size of the laser spot, which is transversal to that of the laser treatment direction.

## 4 Conclusion

The proposed methodology has shown that it is possible to physically simulate with a Gleeble system the severe thermal cycles induced in thin sheet metals by laser heat treatments, thanks to an adequate shaping of a flat Gleeble specimen. A FE thermoelectric model developed to simulate the Gleeble test showed that it is possible to increase the cooling rate to the LHT characteristic values, reducing the width and the length of the shaped area of the specimen. However, the FE model

shows that the increase in cooling rate is related by an increase of the temperature gradient in the shaped area.

The methodology has been applied for the local softening of the EN AW 5754 H32 work-hardened aluminum alloy sheet of 1.5 mm thickness; softening was evaluated by micro-hardness tests. Thermal cycles investigated were obtained by $CO_2$ laser surface treatments, changing thermal cycle peak temperature, interaction time, and shape. The shape of the thermal cycle was modified changing the treatment mode (continuous or pulsed) and the sample geometry laser heat treated. In the range of process parameters explored, results showed that:

The physical simulation is able to predict the softening obtained in a laser surface treatment when thermal cycles and thermal gradients imposed in the specimen are comparable with those of the laser treatment.

Independently from the interaction time and shape of the thermal cycle, the maximum softening is reached when the peak temperature of the thermal cycle reaches values higher than 450 °C.

Independently from the thermal cycle shape, the softening level increases with the increasing of the laser-material interaction time; in fact by increasing the interaction time and by reducing the cooling rate the recovery, recrystallization and grain growth phenomena in the material become more evident.

When the laser heat treatment is performed in pulsed mode and with a spot size equal to the width of a rectangular sample, softening values comparable with that of a full annealing has been observed for interaction times of at least 6 s.

Using the FE thermal model developed for the simulation of the two different laser treatments investigated, a process window relating the peak temperature of the thermal cycle to the laser treatment parameters was obtained. Combining these results with the softening ones obtained by applying the

proposed approach, the softening value of the material can be estimated as a function of laser power and interaction time. Results obtained shows that:

> In correspondence of a treatment mode and interaction time, there is a threshold laser power that must be exceeded in order to have the maximum softening of the aluminum alloy.
> For laser powers above the threshold laser power, the softening level remains constant.
> A reduction in the interaction time of the laser treatment leads to an increase of the threshold laser power.

# References

1. Gunnarsdóttir SA, Basurto AR, Wärmefjord K, Söderberg R, Lindkvist L, Albinsson O, Wandebäck F, Hansson S (2016) Towards simulation of geometrical effects of laser tempering of boron steel before self-pierce riveting. Procedia CIRP 44:304–309

2. Merklein M, Nguyen H (2010) Advanced laser heat treatment with respect for the application for Tailored Heat Treated Blanks. Phys Procedia 5:233–242

3. Piccininni A, Guglielmi P, Franco AL, Palumbo G (2017) Stamping an AA5754 train window panel with high dent resistance using locally annealed blanks. J Phys Conf Ser 896(1):012095 IOP Publishing

4. Merklein M, Böhm W, Lechner M (2012) Tailoring material properties of aluminum by local laser heat treatment. Phys Procedia 39: 232–239

5. Merklein M, Vogt U (2007) Enhanced formability of aluminum blanks by local laser heat treatment. In Proceedings of the 5th international conference on laser assisted net shape engineering (LANE), Erlangen, Germany (pp 1279–1288)

6. Liu W, Lu F, Yang R, Tang X, Cui H (2015) Gleeble simulation of the HAZ in Inconel 617 welding. J Mater Process Technol 225: 221–228

7. Gáspár M, Balogh A, Lukács J (2017) Toughness examination of physically simulated S960QL HAZ by a special drilled specimen. In: Vehicle and Automotive Engineering. Springer, Cham, pp 469–481

8. Wang QF, Shang CJ, Fu RD, Wang YN, Chen W (2005) Physical simulation and metallurgical evaluation of heat-affected zone during laser welding of ultrafine grain steel. Mater Sci Forum 475: 2717–2720 Trans Tech Publications

9. Gleeble® Users Training 2012. Gleeble systems and applications, Spring 2012. DSI: 120419

10. Pasquale Guglielmi, Vincenzo Domenico Lorusso, Maria Emanuela Palmieri, Luigi Tricarico (2019) Physical simulation of laser-induced softening of a high strength aluminum alloy sheet. XIV Convegno dell'Associazione Italiana Tecnologie Manifatturiere AITEM

11. Poole WJ, Militzer M, Wells MA (2003) Modelling recovery and recrystallisation during annealing of AA 5754 aluminium alloy. Mater Sci Technol 19(10):1361–1368